Published in final edited form as:
ACS Chem Biol. 2014 February 21; 9(2): 433–442. doi:10.1021/cb4006886.

Inhibiting AMPylation: A novel screen to identify the first small molecule inhibitors of protein AMPylation‡

Daniel M. Lewallen[1], **Anju Sreelatha**[2], **Venkatasubramanian Dharmarajan**[3], **Franck Madoux**[4], **Peter Chase**[4], **Patrick R. Griffin**[3], **Kim Orth**[2], **Peter Hodder**[4], and **Paul R. Thompson**[1,5,*]

[1]Department of Chemistry, The Scripps Research Institute, Scripps Florida, 120 Scripps Way, Jupiter, Florida 33458

[2]Department of Molecular Biology, UT Southwestern Medical Center, Dallas, TX 75390

[3]Department of Molecular Therapeutics, The Scripps Research Institute, Scripps Florida, 120 Scripps Way, Jupiter, Florida 33458

[4]Lead Identification, The Scripps Research Institute, Scripps Florida, 130 Scripps Way, Jupiter, Florida 33458

[5]The Kellogg School of Science and Technology, The Scripps Research Institute, Scripps Florida

Abstract

Enzymatic transfer of the AMP portion of ATP to substrate proteins has recently been described as an essential mechanism of bacterial infection for several pathogens. The first AMPylator to be discovered, VopS from *Vibrio parahaemolyticus*, catalyzes the transfer of AMP on to the host GTPases Cdc42 and Rac1. Modification of these proteins disrupts downstream signaling events, contributing to cell rounding and apoptosis, and recent studies have suggested that blocking AMPylation may be an effective route to stop infection. To date, however, no small molecule inhibitors have been discovered for any of the AMPylators. Therefore, we developed a fluorescence-polarization based high-throughput-screening assay and used it to discover the first inhibitors of protein AMPylation. Herein we report the discovery of the first small molecule VopS inhibitors (e.g. calmidazolium, GW7647 and MK886) with K_is ranging from 6–50 μM and upwards of 30-fold selectivity versus HYPE, the only known human AMPylator.

INTRODUCTION

Vibrio infections, a main cause of food poisoning, increased 115% between 1998 and 2010.[1, 2] While Vibrio gastroenteritis is typically self-limiting, antibiotic intervention is required in at-risk patients with an underlying medical condition. *Vibrio parahaemolyticus*, the main bacterial cause of this sickness, uses a Type III secretion system to inject host cells

‡This work is supported by funds provided by TSRI to P.R.T. and NIH grants R01-AI056404 to K.O., GM084041 to P.G. and MH084512 to P.H. K.O. and A.S. are supported by Grant I-1561 from the Welch Research Foundation.

*To whom correspondence should be addressed: Department of Chemistry, The Scripps Research Institute, Scripps Florida, 130 Scripps Way, Jupiter, Fl, 33458 tel: (561)-228-2860; fax: (561)-228-2918; Pthompso@scripps.edu.

Supporting Information Available: This material is available free of charge *via* the Internet.

ASSOCIATED CONTENT

Supporting Information

Supplemental Figures 1 to 11 including detailed figure legends as well as full methods for the PAD4 counterscreen, VopS kinetic assays, differential HDX and compound synthesis are in the Supporting Information. This material is available free of charge via the Internet at http://pubs.acs.org.

with effector proteins including VopS. As recently identified by Orth and colleagues,[3] VopS catalyzes the transfer of the AMP portion of ATP to threonine residues present in the host GTPases Cdc42 and Rac1. As a result, this posttranslational modification (PTM) disrupts downstream signaling events eventually leading to cell rounding and apoptosis.[3]

Enzymatic transfer of the AMP portion of ATP to substrate proteins, coined AMPylation, has since been shown to be an essential mechanism for infections caused by *V. parahaemolticus, H. somni*[4] and *Legionella pneumophila*,[5] suggesting that AMPylators are potential therapeutic targets. Supporting this notion is the recent demonstration that antibodies targeting the Fic domain of IbpA from *H. somni* block AMPylation and prevent infection.[6, 7] The fact that several bacterial pathogens including *Klebsiella pneumoniae, Salmonella enterica, Shigella dysenteriae*, and *Mycobacterium tuberculosis* all harbor genes encoding AMPylators further suggests that inhibitors targeting these enzymes may possess broad therapeutic utility.[3–5, 8–17] Additionally, AMPylation is important for eukaryotic cell signaling because deletion of the Fic-domain containing protein in Drosophila leads to blindness.[18] To date, however, no small molecule AMPylator inhibitors have been discovered. Therefore, we set out to develop a high throughput screen (HTS) to identify inhibitors of protein AMPylation.

The basis of our assay platform is the enzyme catalyzed transfer of a fluorophore to a protein substrate, which results in an increase in fluorescence polarization (FP) (Figure 1). In the presence of an inhibitor, however, fluorophore transfer is blocked and there is no increase in FP.[19] We recently identified Fl-ATP as a fluorescently-tagged ATP analogue that is compatible with this type of HTS assay (Figure 1C). Briefly, the k_{cat}/K_M of Fl-ATP is only 10-fold lower than ATP (1.0×10^4 versus 1.2×10^5 $M^{-1}s^{-1}$ for Fl-ATP and ATP, respectively), and we verified that this fluorescent nucleotide is transferred to VopS substrates.[20] Given the high catalytic efficiency of Fl-ATP, we used this analog as the fluorescence source for our FP-based HTS assay, which monitors the VopS catalyzed transfer of Fl-AMP to Cdc42. Using this assay, we identified the first inhibitors of protein AMPylation.

RESULTS AND DISCUSSION

Assay design

We hypothesized that Fl-ATP could be used in a FP-based HTS assay, wherein the VopS catalyzed transfer of Fl-ATP to Cdc42 leads to a time-dependent increase in FP (Figure 1). The principle behind this assay is that when plane polarized light is passed through a sample, Fl-ATP will minimally emit polarized light (because the probe rotates rapidly in solution). When transferred to a protein substrate, the protein-fluorophore complex rotates more slowly, resulting in an observable increase in the emission of polarized light, i.e. FP. Key advantages of this assay format are that the read out is homogenous and requires no washing. Additionally, the assay directly measures inhibitory potency, and the same probes can be used to validate the inhibitors in a gel-based screen.

As opposed to a direct competition assay, as occurs in FP-ABPP assays,[21–23] an additional advantage of our HTS format comes from the fact that since it is an enzymatic assay, it will identify compounds that inhibit enzyme activity regardless of whether they are ATP competitive, prevent protein substrate binding, or are allosteric inhibitors. Note that while the binding of Fl-ATP to the AMPylator itself could also increase the FP signal, preliminary studies indicate that this scenario does not occur with VopS, likely due to the fact that the K_M of VopS for ATP is relatively high (~50 μM).[13, 20] Also note that even if Fl-ATP does bind tightly to the enzyme, we are simply biasing the results of the screen towards compounds that bind to the ATP binding pocket.

Initial assay optimization

To provide the initial proof of concept for this assay, we identified the conditions that would yield a robust time dependent increase in FP (Figure 1D). Initially, the nonionic surfactant pluronic acid (0.01%) was added to our traditional VopS AMPylation buffer to eliminate any false positives that may be due to non-specific aggregation.[24] We then optimized the concentrations of VopS and substrates to achieve a linear response over several hours, as well as provide suitable signal to baseline (S/B) and Z' factors, a measure of assay variability, and be amenable to 384-well plate processing. Both Fl-ATP and Cdc42 concentrations are sub K_M (0.005× and 0.02× respectively) ensuring our ability to identify inhibitors capable of binding at either site. From these experiments (Figure 1D), we identified the ideal concentrations of VopS (0.02 μM), Fl-ATP (0.25 μM) and Cdc42 (5 μM) that provide both a linear response and suitable S/B (~3) and Z' values (~0.8) at 3 h. Note that the 3 h time point was chosen to both maximize S/B and Z' and minimize the number of concurrent robotic handling steps.

Plate-to-plate and day-to-day variability

These optimized conditions were then used to examine the reproducibility of the assay on full 384-well plates using both a DMSO source plate and a control plate. Both the control plate and source plate were pin-transferred (20 nL) into a black 384-well microtiter plate that already contained VopS or no enzyme controls. After pre-incubating for 20 min, both Cdc42 and Fl-ATP were added. A pre-incubation time of 20 min was chosen to allow for the discovery of slow-tight binding inhibitors during the actual screen. ATP was also tested as a low control because this is the normal substrate for the enzyme and effectively acts as an inhibitor by outcompeting binding by Fl-ATP. A random well plot (Figure S1A) shows the clear separation of the high and both low controls. Since ATP and the no VopS columns provided suitable results, the no VopS columns were used for all future Z' calculations. Also, as can be seen in the well scatter plot, we identified zero false positives. A correlation plot (Figure S1B) shows that there was strong repeatability and clustering of the controls and the DMSO sample field. Z' factors were excellent, ~0.8 for each plate (Figure S1C), and the S/B was near 3, indicating this assay is highly reproducible and shows very little deviation in the controls.

Assay reproducibility

To further gauge the sensitivity and reproducibility of the assay, we determined the IC_{50} for the natural substrate, ATP, which inhibits the increase in FP by out competing Fl-ATP. For these studies, 7 replicates of 1/3 dilutions of ATP were pin transferred into the wells and the FP monitored at 0, 30, 60, 120, and 180 min, using the optimized conditions described above (0.02 μM VopS, 0.250 μM Fl-ATP and 5 μM Cdc42) (Figure S2). All replicates showed strong correlations and we obtained good agreement in the IC_{50} values obtained for ATP ($IC_{50(ATP)}$ = 7.0 ± 1 μM) at 3 h. The IC_{50} values obtained at the different time points were also identical within error (6.8 – 7.0 ± 1 μM at 1, 2, and 3 h for ATP), further demonstrating that the 3 h time point provides an acceptable point at which to measure changes in FP.

LOPAC Screen

With an optimized and validated assay in hand, we screened the 1,280-compound LOPAC library (Sigma-Aldrich Library Of Pharmacologically Active Compounds) at 11 μM using the conditions and controls outlined above. A randomized-well activity scatter plot (Figure 2A) of the compounds shows a large assay window, i.e. separation between the controls (Figure 2B: average Z' of 0.89 for the whole assay) and several potential inhibitors in-between. Using a typical assay cut-off,[25] the hit rate was calculated to be 0.4%. While a

small subset of the wells did show negative inhibition, this phenomenon was not reproducible. Therefore, these wells were considered artifacts. Comparing two replicates of the same LOPAC source plate (Figure 2C) demonstrates the reproducibility of the assay (R^2 = 0.72). The structures of the top 5 hits are depicted in Figure 3A.

Counterscreen

We next used our PAD4 FP-ABPP HTS assay as a counterscreen,[22] reasoning that since PAD4 and VopS operate by drastically different mechanisms any compounds that show inhibition are false positives that decrease FP by fluorescence quenching, aggregation or some other non-specific means.[26] Here, we used fluorescein-conjugated F-amidine (FFA),[27] a PAD targeted ABPP that modifies a cysteine residue present in the PAD4 active site, and confirmed that it leads to a time-dependent increase in FP upon incubation with PAD4 (Figure S3). We observed a robust Z' factor (~0.7) and S/B (~6) when using the no enzyme wells as the high control. Also, as can be seen in the well-scatter plot, the level of inhibition by Cl-amidine is an excellent indicator that the assay behaves identically to our previous screen,[22] which used a rhodamine-based fluorophore.

Since none of the top 5 compounds inhibit PAD4 in the counterscreen, we reasoned that they were likely bona fide VopS inhibitors (Figure 3C). Concentration response curves (CRCs) were then generated to confirm that this is the case (Figure 3B). In all cases, dose dependent inhibition of the top hits was observed with IC_{50} values ranging from 11–60 μM. While the ATP analogue Ap4A, is most likely an alternative substrate, the other inhibitors have unique non-ATP like structures, which indicates that it is possible to screen large collections of compounds to identify unique chemotypes for this class of enzyme.

Secondary screens and inhibitor validation

To further confirm that the top hits block Fl-AMP transfer, as opposed to a non-specific effect on the FP signal, we developed a gel-based version of our primary screen. In this screen, if the inhibitors merely interfere with FP and do not block transfer, fluorescently-labeled Cdc42 will still be detected since the inhibitor is removed during the electrophoresis stage of the assay; changes in fluorescence are directly monitored *in gel*. Similar secondary screens have been described.[21, 28] An additional benefit of this assay comes from the fact that it is possible to quantify changes in fluorescence intensity, and thereby provide a semi-quantitative read-out of inhibitor potency. Here, VopS was treated with 10 μM of inhibitors **1–5** before adding sub K_M concentrations of Fl-ATP and Cdc42. After electrophoresis, strong labeling was seen in the control DMSO lane, but there was a decrease in labeling for compounds **1, 3, 4**, and **5** confirming that they do in fact inhibit Fl-AMP transfer to Cdc42 (Figure 4A, Table 1). In contrast, compound **2** appears to be a false positive as it shows only 3% inhibition in this assay.

To gauge selectivity versus other Fic domain containing proteins, we adapted this gel-based assay for HYPE, the only human Fic domain containing protein. Identifying inhibitors that preferentially inhibit VopS over HYPE is important for limiting the potential toxicity of novel VopS targeted therapeutics. For these studies, our HYPE Fic E234G construct was treated analogously to VopS but instead of using Cdc42 as a substrate, we used histone H3 (Figure 4B, Table 1). The HYPE Fic E234G mutant is constitutively active[8] and we recently identified H3 as a HYPE substrate (Figure 4B). Based on this assay, compound **4** shows the highest selectivity (32-fold selective) (Figure 4C), indicating that our screen can discover inhibitors that are specific for bacterial versus human Fic domain containing proteins. The selectivity for VopS over HYPE further indicates that inhibition is not due to a non-specific mechanism.

Inhibitor kinetics

After confirming that four of the top five compounds inhibit VopS in both the primary HTS assay and the gel-based secondary screen, we used our continuous pyrophosphate detection assay to determine modes of inhibition for **1, 3**, and **5**. Inhibitor **4** interfered with the downstream enzymes in the continuous assay, so a radioactive α^{33}P-ATP assay was used for this compound. Based on the Lineweaver-Burk plots and an analysis of the errors, inhibitors **1** and **3** are non-competitive with respect to both Cdc42 and ATP with K_{ii} values of 20 ± 1 and 50 ± 6 μM respectively (Table 1). Inhibitor **5** is competitive with respect to Cdc42 (K_i = 410 ± 110 μM) and has a mixed pattern of inhibition with respect to ATP (K_{is} = 66 ± 19 μM). Compound **4** is the most potent inhibitor, and is competitive with respect to Cdc42 (K_i = 6 ± 1 μM) and non-competitive with respect to ATP. As expected, the K_i values of **1, 3** and **4** correspond to the IC_{50} values calculated from the CRCs since the concentrations of both substrates are well below K_M in the 384-well assay. Inhibitor **5**, however, showed poor inhibition in this continuous assay, possibly due to solubility issues caused by the farnesyl chain, as such this compound was not used in any further experiments.

Cellular Efficacy

To explore their cellular efficacy, we examined whether compounds **1–4** inhibited cellular AMPylation and cell rounding in VopS transfected cells.[3] Compounds **1** and **3** were evaluated at 10 μM and compound **4** was tested at 5 μM, due to its cellular toxicity.[29] As depicted in Figure 5, compounds **1** and **3** decreased cellular protein AMPylation, as measured by Western Blotting, however, compound **4** did not show a significant decrease. While compound **4** was the most potent inhibitor identified from our screen, its high cellular toxicity likely limits its utility as a VopS inhibitor. Furthermore, while compounds **1** and **3** do decrease the amount of protein AMPylation in cells, they were unable to reverse the cell rounding phenotype induced by VopS overexpression (Figure S4).[3] The inability to prevent the cell rounding phenotype is likely due to the fact that the VopS catalyzed AMPylation reaction is thought to be irreversible in human cells. Thus, without more potent inhibitors, cellular rescue may not be possible.

Structure Activity Relationships

Given the high *in vitro* potency of **4**, we set out to develop a structure activity relationship to identify the critical features that are required for the potent inhibition observed with this compound. Analogues of **4** were either synthesized or obtained from the NCI/DTP Open Chemical Repository[30] (Figure 6). Using the HTS assay, we obtained CRCs and IC_{50} values for **4** and 19 derivatives (Figures 6, S5).

By grouping the analogues according to whether they mimic the eastern or western half of the molecule, it became clear that the eastern biphenyl ring is critical for potency. For example, comparing **9** and **4** shows that the loss of the dichlorophenyl ring decreases potency by more than 100 fold. However, the dichlorophenyl moiety is not absolutely required because some of the potency can be regained with a smaller *N*-alkylation, as can be seen with **24**. This increase in potency is not solely due to the cationic charge acquired from the *N,N* disubstitution, however, since compounds **16, 17** and **22** are poor inhibitors. Examining the northwestern portion of **4**, it is apparent when comparing **6** with **7 – 9** or **10** with **11 – 14** that aryl ethers are much more potent than the aliphatic substituents. The third observation from this series of compounds is that the halogens on the southeastern phenethyl aryl ring are important. For example, the IC_{50}s increase in the **4, 15, 23** series as chlorides are removed from the molecule. The fourth and final feature from this series is the tolerance on the northwestern aryl ring by different halogens. Comparing **18 – 21** shows that regardless of the halogens or substitution pattern on the northwestern ring, there is little

change in potency. This is further confirmed by the minimal changes between **7 – 9** and also between **10** and **13**. Therefore, our next generation of compounds should all share the imidazoline core with a western di-aryl system but there can be a wide variety of modifications on the eastern side, which can be tuned for specificity.

Differential Hydrogen Deuterium Exchange (HDX) mass spectrometry

Since none of the compounds were competitive with ATP, we wished to identify where the inhibitors bind to VopS. Since attempts to co-crystallize the compounds with VopS were unsuccessful, we used HDX-MS to map putative binding sites for **3** and **4**. Briefly, compounds **3** and **4** were incubated with 10 μM of VopSΔ30 at a molar excess of 10:1 or 3:1 (ligand:protein) for 1 h before H/D exchange, quenching, on-column pepsin digestion and analysis by ESI-MS. When compared to apo-VopS, VopS in the presence of **4** (100 μM) shows decreased hydrogen exchange with solvent deuterium in the N-terminal region (VopS 31–63), with VopS residues 58–63 showing highest protection against HDX (Figure 7A, B). Protection to solvent exchange would suggest increased stabilization of this region of the protein upon ligand binding and or decreased accessibility of the protected amide hydrogens to solvent. The same region also showed protection at 30 μM, a 3-fold excess, of **4** (Figure S6), suggesting that **4** binds to the N-terminal region of VopS (in particular residues 59–63). The decreased protection observed for the 30 μM sample may reflect the moderate K_i value for **4**, as it is possible that not all VopS binding sites are saturated at the lower concentration.

It should be noted that large areas of destabilization are observed throughout the rest of the protein (residues 147–387) when using 100 μM **4**, which are not present at the lower concentration. This destabilization could be caused by a) **4** is insoluble at 100 μM in the VopS buffer and it causes the protein to precipitate/un-fold, resulting in destabilization/ increased deuterium uptake. This hypothesis seems less likely because some regions are unchanged (colored grey) or show increased protection (blue/green) at the higher concentration; b) VopS is a multimer in solution and the inhibitor binding leads to monomerization/dimerization and can expose the protein dimerization interfaces to more deuterium exchange; or c) inhibitor binding in the N-terminal subdomain induces a global conformational change in the protein. Although the N-terminal region (i.e., residues 31–63) is distal from the active site (residues 348–356) and a deletion construct lacking the first 75 amino acids is still active, the entire N-terminal subdomain is necessary for full activity.[13] Furthermore, previous studies have suggested that a large conformational change occurs upon substrate binding.[13] Thus, we favor the latter explanation for the increased HDX in the core of the protein upon inhibitor binding.

Using a similar differential HDX approach, we characterized the binding of **3** to VopS (Figure 7A, C). Compound **3**, which is a non-competitive inhibitor of both ATP and Cdc42, also showed increased protection within the N-terminus of VopS (residues 59–75). Furthermore, as we saw with **4**, there is substantial destabilization throughout many regions of the rest of the protein. Taken together, these data suggest either that **3** and **4** bind to the N-terminus of VopS or inhibitor binding induces a dramatic conformational change in this region of the enzyme.

Conclusion

In conclusion, we have developed a FP-based HTS compatible assay that relies on the inherent activity of VopS to transfer AMP to Cdc42. We used this assay to screen the 1,280 member LOPAC library and discovered several potential hits. We further characterized these compounds and found 3 of the top 5 are selective for VopS with K_is in the 6–50 μM range. Compounds **1, 3** and **4** display moderate cellular efficacy via their ability to inhibit

AMPylation in VopS transfected cells. Structure activity relationships also identified the imadazoline core of calmidazolium, **4**, as the key pharmacophore that binds to the N-terminal subdomain of VopS. In total, these studies detail the discovery of the first inhibitors for protein AMPylation and set the stage for the discovery of new and more potent derivatives.

METHODS

VopS HTS Assay Validation

8 μL of VopS Screening Buffer (20 mM HEPES pH 8.0, 100 mM NaCl, 1 mM DTT, 5 mM $MgCl_2$, 0.01% pluronic acid) (column 1) or 8 μL of VopSΔ30 (20 nM final) in Screening Buffer (columns 2–23) were added to a black 384-well microtiter plate (Greiner 784076) using a Beckman Coulter Flying Reagent Dispenser (FRD). Controls (columns 1: DMSO (no VopS, high control); 2: 20 mM ATP (high control); and 23: DMSO (no inhibitors, low control)) and source DMSO (100%) (columns 3–22) were pinned 2× using the 10 nL head on a Beckman Coulter BioMek NXP to achieve a final concentration of 0.4% v/v. After a 20 min incubation, 2 μL of substrates, that is Cdc42Q61L (5 μM final) and Fl-ATP (250 nM final) in Screening Buffer, were added using the FRD. The plates were read at 0, 30, 60, 120, 180 and 240 min using a Perkin-Elmer EnVision plate reader (Filters: Ex: FITC FP 480, Em 1: FITC FP P-pol 535, Em 2: FITC FP S-pol 535).

LOPAC Screen

8 μL of VopS Screening Buffer (column 1) or 8 μL of VopSS30 (20 nM final) in Screening Buffer (columns 2–23) were added to a black 384-well microtiter plate (Greiner 784076) using the FRD. Controls (columns 1: DMSO (no VopS, high control); 2: 20 mM ATP (high control); and 23: DMSO (no inhibitors, low control)) and LOPAC molecules (columns 3–22) were pinned 2× using the 10 nL head on a Beckman Coulter BioMek NXP to achieve a final concentration of 11 μM. After a 20 min incubation, 2 μL of substrates (Cdc42Q61L (5 μM final) and Fl-ATP (250 nM final)) in Screening Buffer were added using the FRD. The plates were read after 3 h as described above.

Compound Response Curves (CRC)

8 μL of VopS Screening Buffer (column 1) or 8 μL of VopSΔ30 (20 nM final) in Screening Buffer (columns 2–23) were added to a black 384-well microtiter plate (Greiner 784076) using the FRD. Controls (columns 1: DMSO (no VopS, high control); 2: 20 mM ATP (high control); and 23: DMSO (no inhibitors, low control)) and CRC molecules (columns 3–22) were pinned using the 100 nL head on a Beckman Coulter BioMek NXP to achieve a final concentration of 2 nM to 50 μM. After a 20 min incubation, 2 μL of substrates (Cdc42Q61L (5 μM final) and Fl-ATP (250 nM final)) in Screening Buffer were added using the FRD. The plates were read after 3 h as described above. For each test compound, percent inhibition was plotted against compound concentration. To calculate the IC_{50}, the data were fit to eq. 1,

$$y=((Y_{max}*[I]^n)/(IC_{50}{}^n+[I]^n))+Y_{min} \quad (1)$$

where Y_{max} is the maximum signal, I is the concentration of compound, n is the Hill slope, IC_{50} is the inflection point concentration and Y_{min} is the baseline response using Assay Explorer software (Accelrys Inc). In cases where the highest concentration tested (i.e., 58.6 μM) did not result in greater than 50% inhibition, the IC_{50} was determined manually as greater than 58.6 μM.

Gel-based secondary screens

VopS (20 nM final) was preincubated with inhibitor (10 μM final) in VopS Screening Buffer for 20 min. Cdc42Q61L (5 μM final) and Fl-ATP (1 μM final) were then added. After 15 min, 6× SDS-PAGE loading buffer was added to quench the reaction. The proteins were then separated on a 12% SDS-PAGE gel and imaged to 50 μm on a Typhoon 9410 (GE Healthcare) set at 532 nm. The fluorescent intensities were quantified using Image Quant. Percent inhibition was calculated by normalizing the fluorescence relative to the DMSO control.

HYPE Fic E234G (2.5 μM final) was preincubated with inhibitor (10 μM final) in VopS Screening Buffer for 20 min. Histone H3 (30 μM final) and Fl-ATP (5 μM final) were then added. After 20 min, 6× SDS-PAGE loading buffer was added to quench the reaction. The proteins were then separated on a 12% SDS-PAGE gel and imaged to 50 μm on a Typhoon 9410 (GE Healthcare) set at 532 nm. The fluorescent intensities were quantified using Image Quant. Percent inhibition was calculated by normalizing the fluorescence relative to the DMSO control.

Cell based inhibition assay

HeLa cells (1.5×10^5 cells/well) were seeded in a 6 well plate and grown overnight in DMEM supplemented with 10% fetal bovine serum (Sigma), 2 mM L-glutamine, 100 μg/mL streptomycin, 100 U/mL penicillin, 0.1 mM non-essential amino acids, and 1 mM sodium pyruvate (Invitrogen) at 37 °C with 5% CO_2. The cells were transfected with 100 ng pcDNA3-VopS, 200 ng pGFP-n1 and empty vector pcDNA3 to a total of 2 μg of DNA/well using XtremeGene Hp (Roche). Compounds (5 μM calmidazolium, 10 μM GW7647 or 10 μM MK886) were added to the cells with the transfection reagents. After 6 h, the cells were washed with fresh DMEM and inhibitors were re-added. 18 h post transfection, the cells were fixed using 3.2% paraformaldehyde in 1× PBS for 10 min at room temperature. The fixed cells were imaged using Zeiss LSM 510 confocal microscope. Images were processed using ImageJ and Adobe Photoshop. Alternatively, 18 h after transfection, the cells were harvested in PBS using a cell scraper. The cells were spun down, washed and 50 μL lysis buffer (50 mM Tris, 150 mM NaCl, 1% TX-100, Roche mini protease inhibitor tablet) was added and incubated for 10 min on ice. 5× SDS-PAGE loading buffer was added to the cleared cell lysate, boiled for 10 min and the proteins separated on a 17% SDS-PAGE gel. Proteins were then transferred to PVDF membrane and blocked with 5% milk. Membranes were blotted with rabbit anti-VopS,[3] mouse anti-GFP (BD Biosciences), mouse anti-actin (Sigma) and rabbit anti-AMP-threonine.[31] Percent inhibition was calculated by normalizing the AMP-T band intensity to the VopS band intensity.

Differential Hydrogen deuterium exchange (HDX) Mass Spectrometry

VopSΔ30 (10 μM) was mixed with a 1:3 or 1:10 (protein:ligand) molar excess of calmidozolium (**4**), and MK886 (**3**), and incubated for 1 h at 4 °C for complex formation before subjecting to HDX. For the differential HDX experiments, 5 μL of VopSΔ30 with or without compound were mixed with 20 μL of D_2O-containing HDX buffer (20 mM HEPES pH 8.0, 150 mM NaCl, 1 mM EDTA) and incubated at 4 °C for 0, 10, 30, 60, 90 or 3,600 s and analyzed as previously described.[32]

Supplementary Material

Refer to Web version on PubMed Central for supplementary material.

Acknowledgments

We thank P. Baillargeon and L. DeLuca (Lead Identification, Scripps Florida) for LOPAC screen compound management. K.O. is a Burroughs Welcome Investigator in Pathogenesis of Infectious Disease, a W.W. Caruth, Jr. Biomedical Scholar and has an Earl A. Forsythe Chair in Biomedical Science.

ABBREVIATIONS

AMP	adenosine monophosphate
ATP	adenosine triphosphate
MeCN	acetonitrile
PP_i	inorganic pyrophosphate
HEPES	*N*-(2-hydroxyethyl)piperazine-*N*'-(2-ethanesulfonic acid)
EDTA	ethylenediamine tetraacetic acid
CRC	compound response curves
MALDI	matrix-assisted laser desorption/ionization
DTT	dithiothreitol
Fl-ATP	N6-(6-amino)hexyl-ATP-5-carboxyl-fluorescein
Fl-AMP	N6-(6-amino)hexyl-AMP-5-carboxyl-fluorescein
FFA	fluorescein tagged F-amidine.

References

1. Scallan E, Hoekstra RM, Angulo FJ, Tauxe RV, Widdowson MA, Roy SL, Jones JL, Griffin PM. Foodborne illness acquired in the United States--major pathogens. Emerg Infect Dis. 2011; 17:7–15. [PubMed: 21192848]
2. (Cdc), C. f. D. C. a. P. Vital Signs: Incidence and Trends of Infection with Pathogens Transmitted Commonly Through Food --- Foodborne Diseases Active Surveillance Network, 10 U.S. Sites, 1996–2010. MMWR. Morbidity and Mortality Weekly Reports. 2010. Retrieved from http://cdc.gov/mmwr/preview/mmwrhtml/mm6022a6025.htm?s_cid=mm6022a6025w
3. Yarbrough ML, Li Y, Kinch LN, Grishin NV, Ball HL, Orth K. AMPylation of Rho GTPases by Vibrio VopS Disrupts Effector Binding and Downstream Signaling. Science. 2009; 323:269–272. [PubMed: 19039103]
4. Worby CA, Mattoo S, Kruger RP, Corbeil LB, Koller A, Mendez JC, Zekarias B, Lazar C, Dixon JE. The Fic Domain: Regulation of Cell Signaling by Adenylylation. Mol Cell. 2009; 34:93–103. [PubMed: 19362538]
5. Müller MP, Peters H, Blümer J, Blankenfeldt W, Goody RS, Itzen A. The Legionella effector protein DrrA AMPylates the membrane traffic regulator Rab1b. Science. 2010; 329:946–949. [PubMed: 20651120]
6. Geertsema RS, Worby C, Kruger RP, Tagawa Y, Russo R, Herdman DS, Lo K, Kimball RA, Dixon J, Corbeil LB. Protection of mice against H. somni septicemia by vaccination with recombinant immunoglobulin binding protein subunits. Vaccine. 2008; 26:4506–4512. [PubMed: 18590787]
7. Geertsema RS, Zekarias B, La Franco Scheuch L, Worby C, Russo R, Gershwin LJ, Herdman DS, Lo K, Corbeil LB. IbpA DR2 subunit immunization protects calves against Histophilus somni pneumonia. Vaccine. 2011; 29:4805–4812. [PubMed: 21557979]
8. Engel P, Goepfert A, Stanger FV, Harms A, Schmidt A, Schirmer T, Dehio C. Adenylylation control by intra- or intermolecular active-site obstruction in Fic proteins. Nature. 2012; 482:107–110. [PubMed: 22266942]

9. Mishra S, Bhagavat R, Chandra N, Vijayarangan N, Rajeswari H, Ajitkumar P. Cloning, expression, purification, and biochemical characterisation of the FIC motif containing protein of Mycobacterium tuberculosis. Protein Expr Purif. 2012; 86:58–67. [PubMed: 22982230]
10. Grammel M, Luong P, Orth K, Hang HC. A chemical reporter for protein AMPylation. J. Am. Chem. Soc. 2011; 133:17103–17105. [PubMed: 21942216]
11. Kinch LN, Yarbrough ML, Orth K, Grishin NV. Fido, a novel AMPylation domain common to fic, doc, and AvrB. PLoS ONE. 2009; 4:e5818. [PubMed: 19503829]
12. Li Y, Al-Eryani R, Yarbrough ML, Orth K, Ball HL. Characterization of AMPylation on Threonine, Serine, and Tyrosine Using Mass Spectrometry. J Am Soc Mass Spectrom. 2011; 22:752–761. [PubMed: 21472612]
13. Luong P, Kinch LN, Brautigam CA, Grishin NV, Tomchick DR, Orth K. Kinetic and structural insights into the mechanism of AMPylation by VopS Fic domain. J Biol Chem. 2010; 285:20155–20163. [PubMed: 20410310]
14. Neunuebel MR, Chen Y, Gaspar AH, Backlund PS, Yergey A, Machner MP. De-AMPylation of the Small GTPase Rab1 by the Pathogen Legionella pneumophila. Science. 2011; 333:453–456. [PubMed: 21680813]
15. Tan Y, Luo Z-Q. Legionella pneumophila SidD is a deAMPylase that modifies Rab1. Nature. 2011; 475:506–509. [PubMed: 21734656]
16. Mattoo S, Durrant E, Chen MJ, Xiao J, Lazar CS, Manning G, Dixon JE, Worby CA. Comparative analysis of Histophilus somni immunoglobulin-binding protein A (IbpA) with other fic domain-containing enzymes reveals differences in substrate and nucleotide specificities. J Biol Chem. 2011; 286:32834–32842. [PubMed: 21795713]
17. Xiao J, Worby CA, Mattoo S, Sankaran B, Dixon JE. Structural basis of Fic-mediated adenylylation. Nature Structural & Molecular Biology. 2010; 17:1004.
18. Rahman M, Ham H, Liu X, Sugiura Y, Orth K, Krämer H. Visual neurotransmission in Drosophila requires expression of Fic in glial capitate projections. Nature Neuroscience. 2012; 15:871.
19. Li Z, Mehdi S, Patel I, Kawooya J, Judkins M, Zhang W, Diener K, Lozada A, Dunnington D. An ultra-high throughput screening approach for an adenine transferase using fluorescence polarization. J Biomol Screen. 2000; 5:31–38. [PubMed: 10841598]
20. Lewallen DM, Steckler CJ, Knuckley B, Chalmers MJ, Thompson PR. Probing adenylation: using a fluorescently labelled ATP probe to directly label and immunoprecipitate VopS substrates. Mol Biosyst. 2012; 8:1701–1706. [PubMed: 22456874]
21. Cravatt BF, Wright AT, Kozarich JW. Activity-based protein profiling: from enzyme chemistry to proteomic chemistry. Annu Rev Biochem. 2008; 77:383–414. [PubMed: 18366325]
22. Knuckley B, Jones JE, Bachovchin DA, Slack J, Causey CP, Brown SJ, Rosen H, Cravatt BF, Thompson PR. A fluopol-ABPP HTS assay to identify PAD inhibitors. Chem Commun (Camb). 2010; 46:7175–7177. [PubMed: 20740228]
23. Zuhl AM, Mohr JT, Bachovchin DA, Niessen S, Hsu KL, Berlin JM, Dochnahl M, Lopez-Alberca MP, Fu GC, Cravatt BF. Competitive Activity-Based Protein Profiling Identifies Aza-beta-Lactams as a Versatile Chemotype for Serine Hydrolase Inhibition. J Am Chem Soc. 2012; 134:5068–5071. [PubMed: 22400490]
24. Ryan AJ, Gray NM, Lowe PN, Chung CW. Effect of detergent on "promiscuous" inhibitors. J Med Chem. 2003; 46:3448–3451. [PubMed: 12877581]
25. Minond D, Saldanha SA, Spicer T, Qin L, Mercer BA, Roush WR, Hodder P. HTS Assay for Discovery of Novel Metallo-Beta-lactamase (MBL) Inhibitors. 2010
26. Luo Y, Knuckley B, Bhatia M, Pellechia PJ, Thompson PR. Activity-based protein profiling reagents for protein arginine deiminase 4 (PAD4): synthesis and in vitro evaluation of a fluorescently labeled probe. J. Am. Chem. Soc. 2006; 128:14468–14469. [PubMed: 17090024]
27. Slack JL, Causey CP, Luo Y, Thompson PR. Development and use of clickable activity based protein profiling agents for protein arginine deiminase 4. ACS Chem Biol. 2011; 6:466–476. [PubMed: 21265574]
28. Knuckley B, Luo Y, Thompson PR. Profiling Protein Arginine Deiminase 4 (PAD4): a novel screen to identify PAD4 inhibitors. Bioorg Med Chem. 2008; 16:739–745. [PubMed: 17964793]
29. Database", N. C. f. B. I. P. B. AID = 588440.

30. http://dtp.cancer.gov

31. Hao YH, Chuang T, Ball HL, Luong P, Li Y, Flores-Saaib RD, Orth K. Characterization of a rabbit polyclonal antibody against threonine-AMPylation. J Biotechnol. 2011; 151:251–254. [PubMed: 21185336]

32. Goswami D, Devarakonda S, Chalmers MJ, Pascal BD, Spiegelman BM, Griffin PR. Time window expansion for HDX analysis of an intrinsically disordered protein. J Am Soc Mass Spectrom. 2013; 24:1584–1592. [PubMed: 23884631]

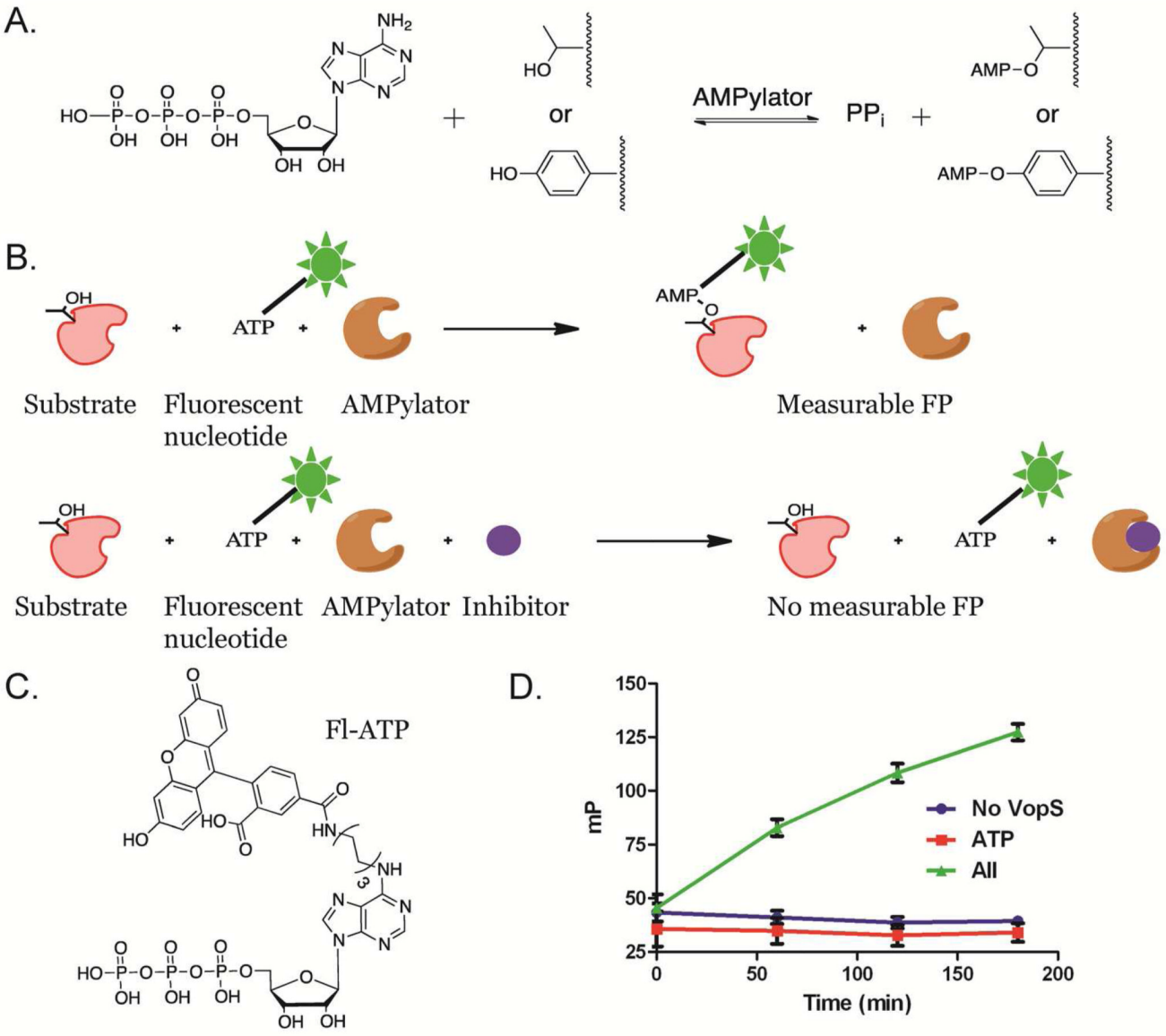

Figure 1.

VopS reaction and assay design. a) AMPylators transfer AMP to side chain threonines or tyrosines. b) FP assay design. A time dependent increase in FP signal occurs as VopS transfers Fl-AMP to Cdc42. In the presence of an inhibitor, however, no Fl-AMP is transferred and the FP signal is diminished. c) Structure of Fl-ATP. d) Substrates (Cdc42 and Fl-ATP) were added to 16 replicates of VopS, VopS with 0.4 mM ATP or VopS Screening Buffer in a 384-well plate. FP was measured as a function of time.

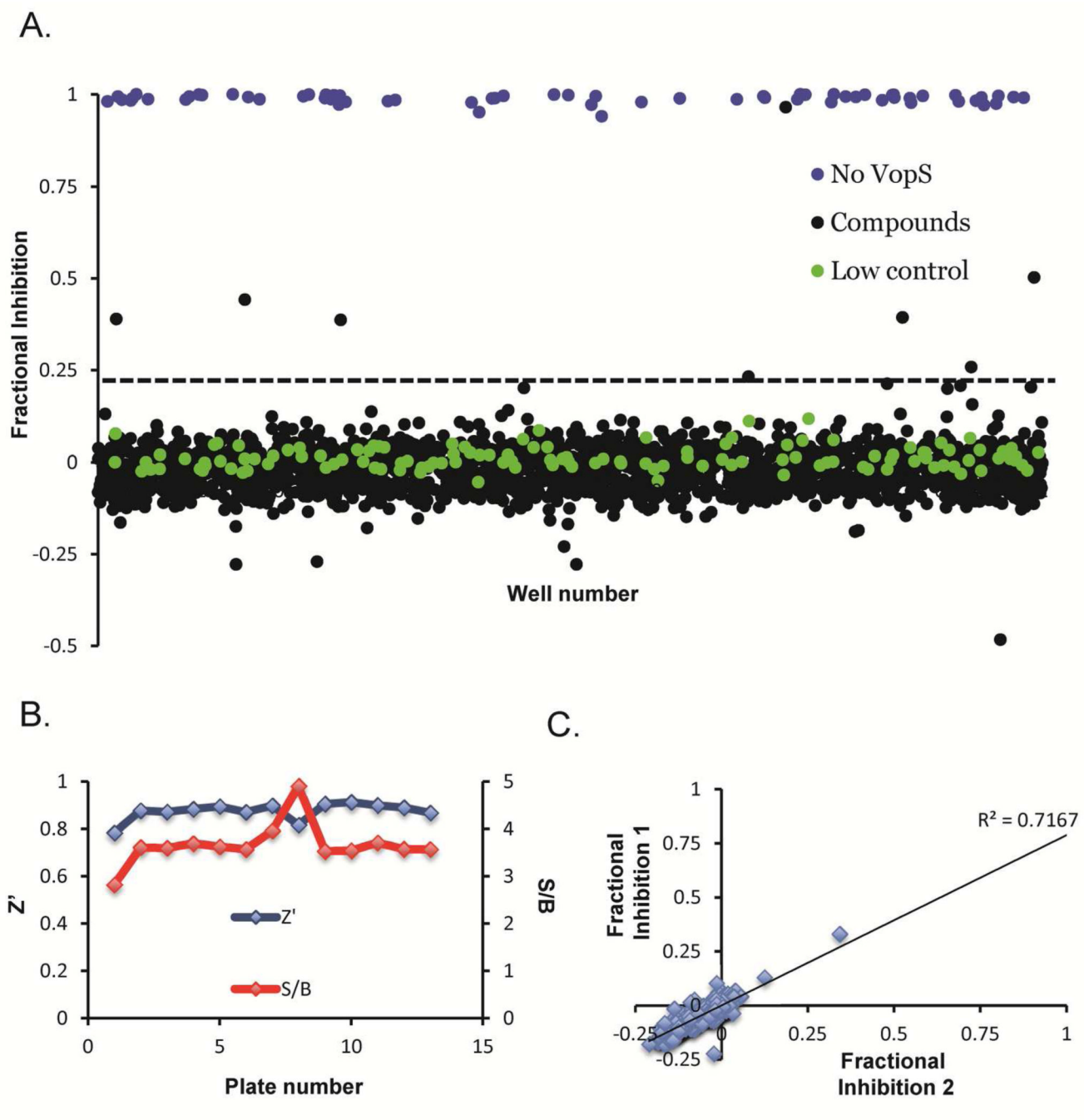

Figure 2.

LOPAC screen. The LOPAC library was screened in triplicate. The compound activity can be seen in a) Random well scatter of the 3 h normalized FP values. Assay quality is shown by b) Z' and S/B plots for each of the 13 plates, and c) Well correlation between 2 of the LOPAC plates.

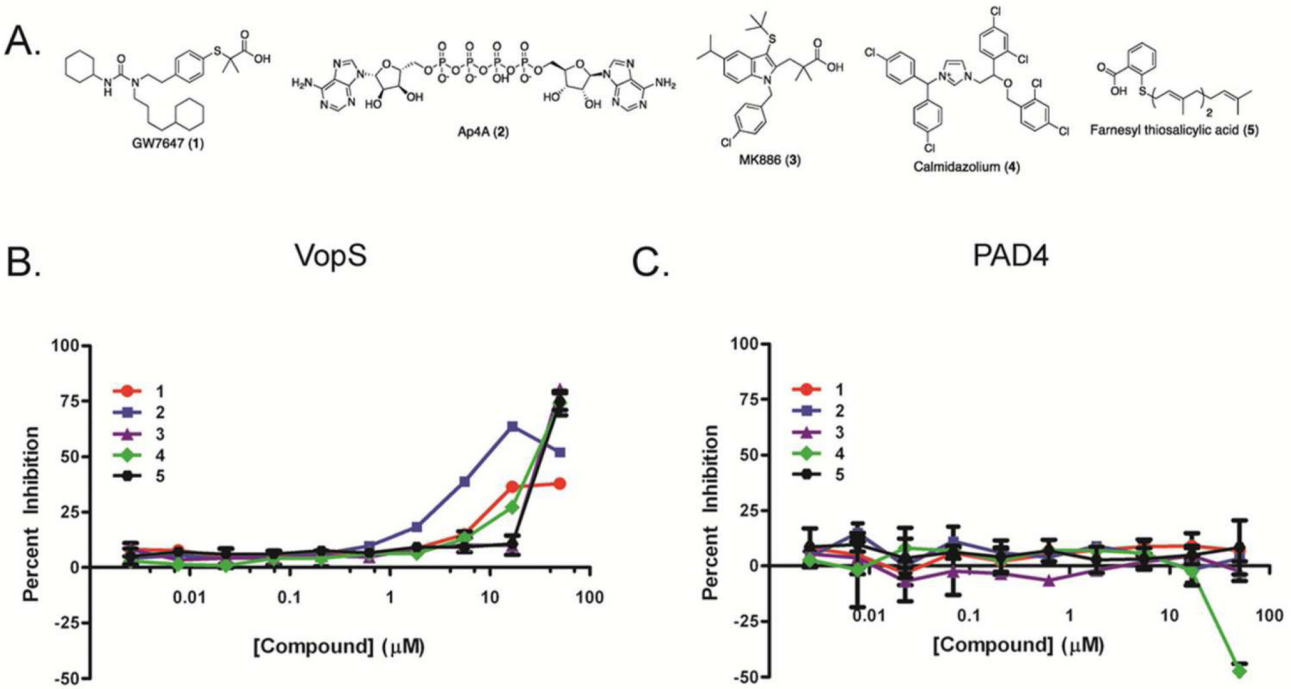

Figure 3.

Hit Validation. a) Structures of the most efficacious 5 hits from the LOPAC screen. Concentration response curves (CRC) for the same compounds with b) VopS and c) PAD4. The CRC for PAD4 were generated using the PAD4 targeted FP-ABPP assay.

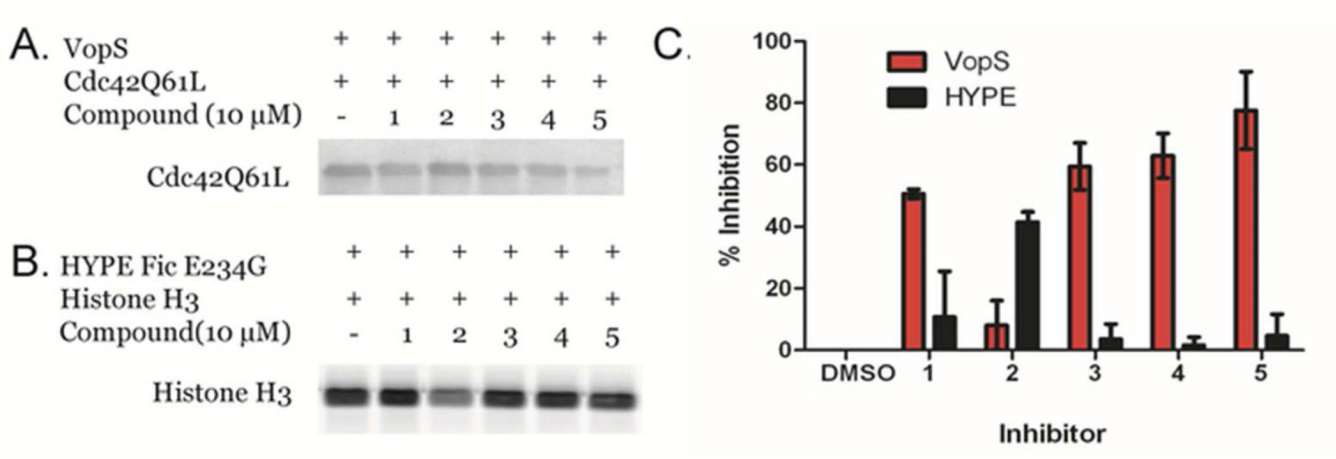

Figure 4.

Gel-based counterscreen. The top five hits from the LOPAC CRC were analyzed using a gel-based assay with a) VopS or b) HYPE Fic E234G. c) Normalized percent inhibition from duplicate data relative to the DMSO control from the gel based screen for both VopS and HYPE Fic E234G.

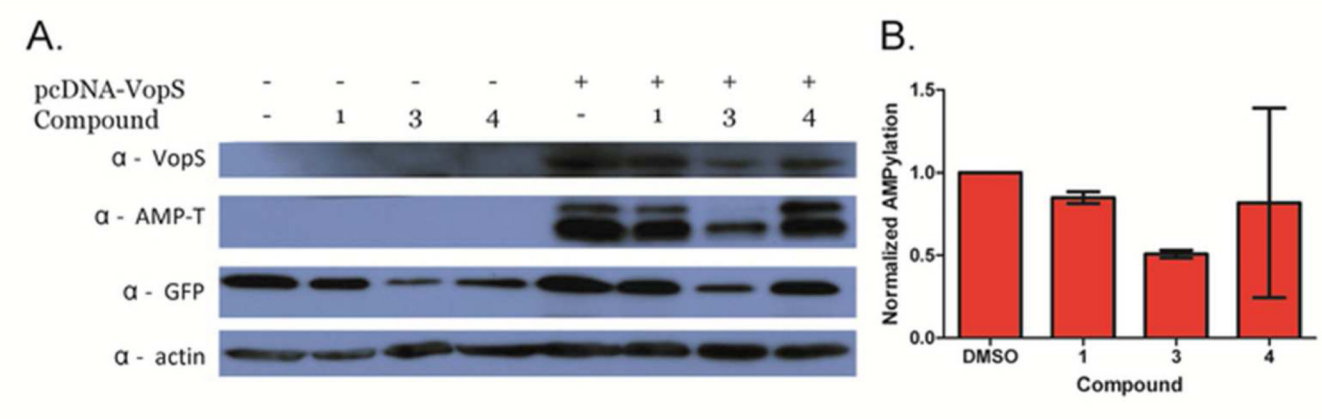

Figure 5.

In cellulo efficacy of validated VopS inhibitors. a) Western blot of the lysates from GFP or VopS/GFP transfected HeLa cells in the presence or absence of compounds **1** (10 μM), **3** (10 μM), or **4** (5 μM). b) Quantified band intensities of the AMP-Threonine blots normalized against VopS.

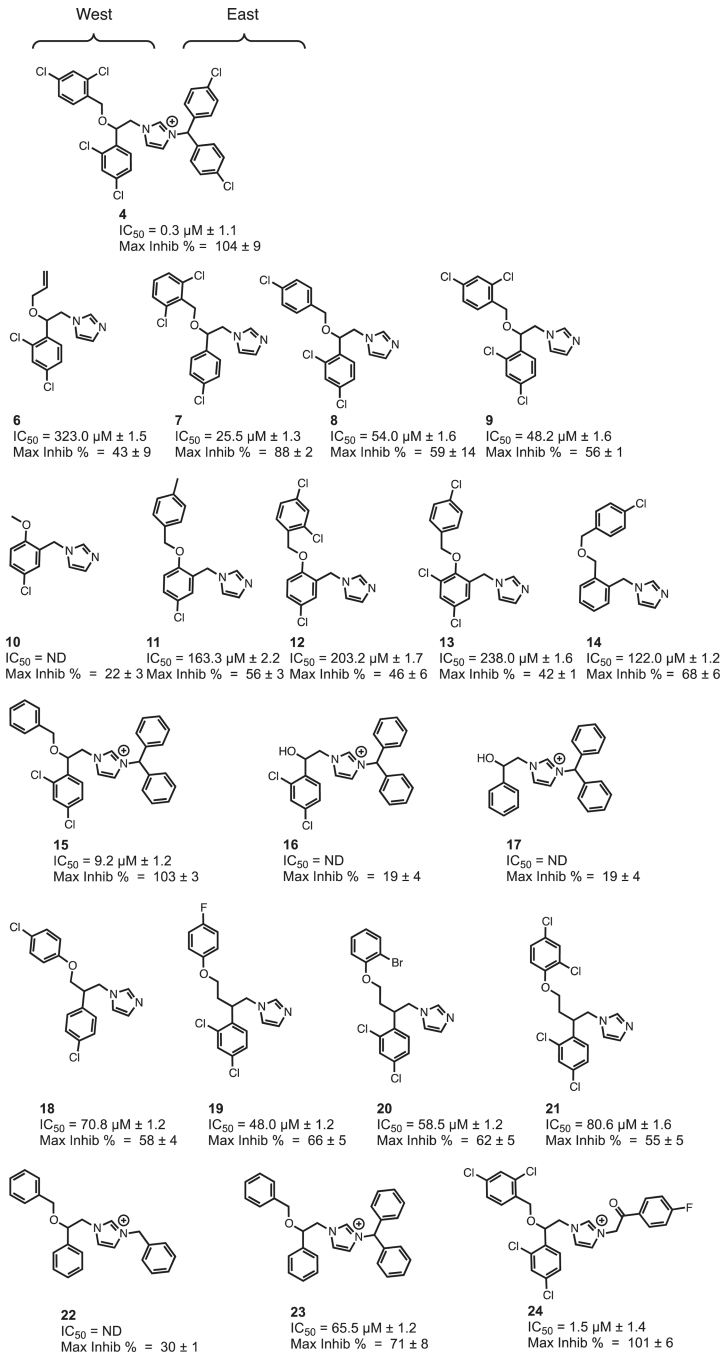

Figure 6.

Calmidazolium derivative characterization. Structures and inhibition values of the calmidazolium derivatives as determined from the CRC screen grouped by their structural differences.

A.

Sequence	Charge	Start	End	Compound 4 (10X)	Compound 3 (10X)
YFQGGSGKEYTINAATQE	2	25	42	-8 (3)	2 (2)
ATQEFTRANPTSGAVARF	3	39	56	-9 (3)	-4 (3)
FTRANPTSGAVARF	3	43	56	-8 (3)	-6 (3)
FEATGKL	1	57	63	-15 (3)	-16 (3)
FREGSTQSVAKAIT	3	64	77	-7 (2)	-5 (3)
FREGSTQSVAKAITKAVF	3	64	81	-3 (2)	-11 (3)
KAITKAVF	2	74	81	-1 (3)	-3 (2)
VFDNEQGQAQRLQTSSSVEHGQML	3	80	103	0 (2)	3 (2)
DNEQGQAQRLQT	2	82	93	-1 (4)	0 (2)
DNEQGQAQRLQTSSSVEHGQML	3	82	103	1 (2)	2 (2)
RLQTSSSVEHGQML	3	90	103	2 (2)	1 (2)
FKDANLKTPSDVL	2	104	116	3 (2)	6 (2)
FKDANLKTPSDVLNA	3	104	118	4 (2)	7 (2)
FAKLDSKM	2	119	126	2 (2)	2 (2)
FAKLDSKMVKSHAAE	3	119	133	0 (2)	0 (2)
FAKLDSKMVKSHAAEL	2	119	134	0 (2)	0 (2)
SQLAERAMTE	2	135	144	3 (1)	8 (1)
SQLAERAMTEVM	2	135	146	3 (0)	3 (1)
AERAMT	2	138	143	4 (1)	10 (1)
AERAMTEVM	2	138	146	3 (0)	9 (1)
VMLETDSGKNLKALIGDD	2	145	162	10 (1)	9 (2)
LETDSGKNLKALIGDD	3	147	162	10 (1)	11 (1)
LETDSGKNLKALIGDDAVKSL	3	147	167	9 (1)	10 (1)
LETDSGKNLKALIGDDAVKSLA	3	147	168	10 (1)	10 (1)
VRVVKDYGGGVAAAQKNPEVRINQM	3	169	193	6 (2)	7 (3)
VRVVKDYGGGVAAAQKNPEVRINQMQ	4	169	194	8 (2)	8 (3)
AAQKNPEVRINQMQ	3	181	194	6 (2)	7 (3)
DMEVMHLKAAQRHIEGL	2	198	214	6 (2)	9 (3)
MEVMHLKAAQRHIEGL	3	199	214	6 (1)	8 (1)
VMHLKAAQRHIEGL	2	201	214	10 (1)	14 (2)
ASTDLNQGVY	1	215	224	4 (3)	9 (3)
ASTDLNQGVYAEGLPEDAF	2	215	233	4 (2)	8 (2)
NQGVYAEGLPEDAF	2	220	233	4 (1)	7 (2)
AEGLPEDAF	1	225	233	2 (1)	5 (3)
AEGLPEDAFNKAGVTNNVERAAA	3	225	247	5 (2)	9 (2)
FNKAGVTNNVERAAA	3	233	247	5 (2)	10 (2)
NKAGVTNNVERAAA	3	234	247	5 (2)	9 (2)
NKAGVTNNVERAAAW	3	234	248	6 (1)	11 (2)
WIINASNSKGND	2	248	259	1 (1)	2 (2)
WIINASNSKGNDAE	2	248	261	1 (2)	3 (2)
WIINASNSKGNDAEN	2	248	262	1 (2)	2 (2)
WIINASNSKGNDAENITSL	2	248	266	2 (2)	4 (2)
WIINASNSKGNDAENITSLL	2	248	267	3 (1)	4 (2)
IINASNSKGNDAENITSL	2	249	266	1 (2)	3 (2)
AENITSL	1	260	266	3 (3)	6 (3)
LKEYATNGKDLL	2	267	278	10 (1)	13 (2)
LKEYATNGKDLLNM	3	267	280	12 (1)	12 (2)
LKEYATNGKDLLNMDNL	3	267	283	6 (1)	5 (1)
KEYATNGKDLLNM	3	268	280	10 (2)	12 (2)
YATNGKDLLNM	2	270	280	10 (1)	12 (2)
YATNGKDLLNMDNL	2	270	283	10 (2)	11 (2)
DNLKELHARLVPNVERD	3	281	297	8 (2)	6 (2)
YRGPNISGGTLPSSIGGEGML	2	298	318	6 (2)	7 (2)
YRGPNISGGTLPSSIGGEGMLKQHIEGF	4	298	325	10 (2)	11 (2)
YRGPNISGGTLPSSIGGEGMLKQHIEGFL	4	298	326	8 (2)	9 (2)
FLKENPVADKDLGKHLFA	3	325	342	8 (1)	9 (2)
LKENPVADKDLGKHLFA	3	326	342	7 (1)	7 (2)
GVIGYHGFTDGNGRM	3	343	357	2 (2)	5 (2)
GRMLYA	2	358	363	1 (1)	5 (1)
YAIAEL	1	362	367	3 (1)	6 (2)
IAELRNDSFNPLAM	2	364	377	10 (1)	13 (2)
IAELRNDSFNPLAMNAENSLHGIK	4	364	387	10 (1)	13 (2)
LRNDSFNPLAM	2	367	377	10 (2)	12 (2)
LRNDSFNPLAMNAENSLHGIK	4	367	387	8 (2)	9 (2)
RNDSFNPLAM	2	368	377	9 (2)	12 (2)
NAENSLHGIK	3	378	387	10 (2)	11 (3)
ENSLHGIK	2	380	387	4 (2)	11 (5)

B.

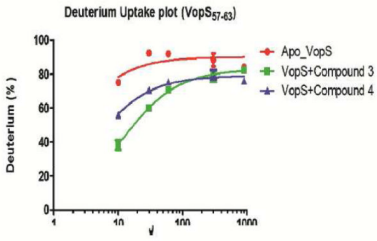

Figure 7.

HDX of VopS with **3** or **4**. a) Heat map of the change in deuterium exchange of VopS incubated with 100 μM **3** or **4** shows protection in the N-terminal region VopS 57–63. b) Deuterium uptake plot for VopS 57–63 shows a time dependent decrease in HDX in the presence of 100 μM **4** or 100 μM **3**.

Table 1

Inhibition values for the HTS

Compound	Primary screen inhibition[a]	CRC IC_{50} VopS (μM)	CRC IC_{50} PAD4 (μM)	Gel based % inhibition VopS[b]	Gel based % inhibition HYPE[b]	Fold selective
1	61% ± 38	>59	>59	55%	10%	6
2	47% ± 4	11	>59	3%	41%	0
3	41% ± 3	50	>59	22%	4%	6
4	33% ± 1	40	>59	63%	2%	32
5	25% ± 1	52	>59	79%	5%	16

[a] Average of three replicates;

[b] 10 μM compound;

Table 2

Mechanism of inhibition values for VopS

Compound	Varied substrate	Mechanism of inhibition	K_{is} (μM)	K_{ii} (μM)
1	Cdc42	Non-competitive		20 ± 1
	ATP	Non-competitive		41 ± 5
3	Cdc42	Non-competitive		99 ± 16
	ATP	Non-competitive		50 ± 6
4	Cdc42	Competitive		6 ± 1
	ATP	Non-competitive		26 ± 4
5	Cdc42	Competitive		410 ± 110
	ATP	Mixed	66 ± 19	310 ± 38